Research Square

Preprints are preliminary reports that have not undergone peer review.
They should not be considered conclusive, used to inform clinical practice,
or referenced by the media as validated information.

Hypoxia-Induced Senescence Drives Immunosuppression in NPC via the MIF-CD74 Axis, an Actionable Therapeutic Target

Taoyuan Xiao
Loudi Central Hospital
Ying Zhang
Loudi Central Hospital
Quan Li
Loudi Central Hospital
Xianfang Chen
Loudi Central Hospital
Fusen Peng
399012439@qq.com

Loudi Central Hospital

Research Article

Keywords: Nasopharyngeal carcinoma, Cellular senescence, Single-cell RNA sequencing, MIF-CD74 axis, Prognostic model

Posted Date: July 14th, 2026

DOI: https://doi.org/10.21203/rs.3.rs-9896268/v1

License: This work is licensed under a Creative Commons Attribution 4.0 International License.
Read Full License

Additional Declarations: No competing interests reported.

Abstract

Background

Cellular senescence within the hypoxic tumor microenvironment is a key contributor to tumor progression and therapy resistance. However, its specific role and regulatory mechanisms in nasopharyngeal carcinoma(NPC) remain poorly characterized at single-cell resolution.

Methods

We analyzed single-cell RNA sequencing data from 15 primary NPC tumors using a Computational Senescence Prediction and Classification Framework (CSPCF) based on XGBoost. Cellular heterogeneity, cell-cell communication, and gene regulatory networks were investigated. The clinical relevance was assessed using Cox regression and drug sensitivity analyses from public databases.

Results

The CSPCF framework successfully classified cellular senescence states, identifying a distinct hypoxic senescent tumor subpopulation (S2) with high proliferative potential and immune evasion capabilities. Cell-cell communication analysis revealed that the MIF-CD74 ligand-receptor axis is a critical mediator between senescent tumor and immune cells. Gene regulatory network analysis identified 33 S2-specific transcription factors, including E2F2, E2F7, and E2F8, which are associated with hypoxia, epithelial-mesenchymal transition, and cell cycle pathways. A prognostic model based on three of these transcription factors (PBX3, FOXP1, and BCLAF1) effectively stratified patients into high- and low-risk groups with significantly different overall survival in both training ($n = 97$, $p < 0.001$) and validation cohorts ($p = 0.046$), independent of clinical variables. Virtual gene perturbation analysis validated the functional roles of key TFs. Additionally, drug sensitivity analysis identified six compounds (including vinblastine, vorinostat, and four additional agents; see Supplementary Table S3) targeting senescence-associated vulnerabilities.

Conclusion

Our study delineated the landscape of hypoxia-induced senescence in NPC, highlighting the pivotal MIF-CD74 axis and a specific transcription factor (TF) network driving tumor aggression and immunosuppression. The identified prognostic signature and therapeutic candidates provide novel insights into improving NPC patient stratification and treatment.

Introduction

Nasopharyngeal carcinoma (NPC) is a malignant tumor of the head and neck with distinct geographical and population correlations and is particularly prevalent in southern China, Southeast Asia, and North Africa[1–2]. Global epidemiological data, including incidence rates, mortality rates, and disability-adjusted life years (DALYs), reveal that NPC poses a significant threat to human health and life, with predictions that the disease burden will peak by 2040[3].

The treatment of NPC is a complex process involving various methods and strategies, such as radiotherapy, chemotherapy, and immunotherapy; radiotherapy is the primary treatment, and chemotherapy (including induction chemotherapy, concurrent chemoradiotherapy, and adjuvant chemotherapy) is an important supplementary measure for recurrence or metastatic disease [5–7]. Despite advancements in intensity-modulated radiotherapy (IMRT), approximately 10% of NPC patients with NPC exhibit resistance to radiotherapy, leading to treatment failure, recurrence, and poor prognosis. Once platinum resistance develops, alternative treatment options are lacking. Limited treatment options are available for recurrent or metastatic disease, and there is an urgent need for further research to explore new therapeutic strategies to improve treatment outcomes and quality of life in these NPC patients [8–10]. Recently, immunotherapy combinations including toripalimab plus anlotinib have shown promise in recurrent or metastatic NPC [28], highlighting the clinical relevance of immune-targeted strategies.

Low tumor oxygenation, also known as hypoxia, is a common characteristic of solid tumors and a key factor in the tumor microenvironment that promotes the spread (invasion) of cancer cells into healthy tissues to evade this adverse microenvironment[11, 12]. Hypoxia is an important factor affecting radiotherapy sensitivity, and several previous studies have reported that hypoxia enhances the migration and invasion of multiple solid tumors by activating specific signaling pathways or regulators, such as HIF-1α, HIF-2α, and the EMT transcription factor ZEB1. Research by Ying Lan et al. found that HIF-1α promotes the proliferation, invasion, and metastasis of NPC cells by regulating the expression of MMP-2, indicating that hypoxia may play a key role in the aggressiveness and metastasis of NPC[13–15]. Therefore, understanding the hypoxic status of the tumor microenvironment can help improve the treatment of nasopharyngeal carcinoma[16–18].

This study aimed to explore the impact of hypoxia on nasopharyngeal carcinoma cells, including immune and tumor cells, and how hypoxia mediates tumor invasion. We first designed a Computational Senescence Prediction and Classification Framework (CSPCF) to predict cellular senescence status and applied it to single-cell RNA-seq data analysis to uncover the landscape of cellular senescence and identify key regulatory factors in hypoxic subpopulations with high invasive potential in NPC, thereby providing new insights for targeted therapy in NPC patients.

Materials and Methods

We downloaded the single-cell RNA transcription data of NPC from GSE150430 in the Gene Expression Omnibus (GEO) database, which included 15 primary NPC tumors and one normal sample [4]. The raw

count expression profiles were normalized and scaled using the Seurat R package. Quality control (QC) filters were applied using mitochondrial RNA and ribosomal gene percentages. Genes expressed in fewer than three cells were excluded. Cells with more than 2.5% mitochondrial counts or more than 20% ribosomal DNA were filtered out. After quality control, 45,325 high-quality cells were retained for downstream analysis.

Identification of high-confidence cells

The gene set that defined senescence was derived from the MSigDB database. The keywords of these gene sets included 12 traits associated with aging, genomic instability, telomere attrition, epigenetic alterations, loss of proteostasis, disabled macroautophagy, deregulated nutrient-sensing, mitochondrial dysfunction, cellular senescence, stem cell exhaustion, altered intercellular communication, chronic inflammation, and dysbiosis. single-sample gene set enrichment assays (ssGSEA) were used to calculate the activity score of each cell in these senescence-related gene sets. For each gene set, Gaussian mixture model (GMM) was used to assign cells into high- and low-score groups based on cell activity scores. Cells were considered high-confidence senescent cells if they were all assigned to the high-score group in the seven GMMs, and cells were considered high-confidence normal cells if they were all assigned to the low-score group in the seven GMMs. The optimal number of GMM components (k = 7) was determined based on the silhouette score and Bayesian Information Criterion (Supplementary Table S1).

Cellular senescent Prediction and Classification Framework (CSPCF)

We used high-confidence cells to predict the senescence status of the other unclassified cells. Differential expression analysis between high-confidence senescent and normal cells was performed using the Wilcoxon rank-sum test, and the top 500 differentially expressed genes (DEGs) were selected as input features. We used the createDataPartition() function in the caret package to split the high-confidence cells into training and test sets. In each training set, XGBoost was used to classify all the cells into normal and senescent groups. To ensure the stability of the model, the final model was built on the training set through 5x cross-validation. The accuracy of the final applied model exceeded 0.85 in both training and test sets.

Cross-talk between tumor cells and immune cells in different senescent states was performed using the CellChat package [31]. The gene expression data of each cell were obtained from the Seurat normalized expression matrix. We identified overexpressed ligands or receptors among cell types, and used the “computeCommunProbPathway” function to infer the cell-cell communication at a signaling pathway level.

Single cell RNA-seq clustering and marker genes identification

We applied the top 2000 highly variable features of the dataset to perform principal component analysis to reduce the dimensionality of the data, and the top 30 principal components were used for downstream analyses. Cell subpopulations were identified using the “FindClusters” function (resolution = 0.9) and visualized using t-SNE. To identify the marker gene for each subpopulation, we used the “FindMarkers” function for each senescent subpopulation and all normal tumor cells.

KEGG and GO enrichment analysis

The R package clusterProfiler was used to perform GO and KEGG enrichment analyses [33, 34]. The Cytoscape plugins EnrichmentMap and AutoAnnotate were used to visualize similar pathways with stringent pathway similarity scores.

Cell status-specific gene regulatory network analysis and critical genes identification

Cell status-specific gene regulatory networks were constructed for the S1 and N3 subpopulations by SCENIC [32]. GENIE3 was used to construct a co-expression network, and RcisTarget was used to identify the regulons for each transcription factor. The importance of the node network was analyzed using Python networkx 2.3. Critical genes were identified using four SNA measures (degree centrality, closeness centrality, pagerank, and betweenness centrality) in each network.

We downloaded two gene expression datasets from GEO (GSE65858 and GSE41613), which contained gene expression data and clinical information [30]. 58 NPC patients from GSE41613 were treated as a training dataset, and 59 Laryngeal and Hypopharyngeal cancer patients from GSE65858 were used as independent validation datasets. We performed univariate Cox proportional hazards regression to investigate the association between the expression of critical TFs and OS of NPC patients in the training set. Significant survival-related genes were selected ($P < 0.05$) to further perform variable selection using stepwise regression analysis. Ultimately, three TFs (PBX3, FOXP1, and BCLAF1) were identified in our study to construct the final prognostic model based on gene expression weighted by regression coefficients of univariable Cox regression analysis.

Patients were classified into high-risk and low-risk groups based on the median risk score. KM curves were used to compare OS between the two groups. Multivariate Cox regression analyses were performed with the risk score and tumor-infiltrating lymphocytes (TILS) as variables to assess whether the risk score could be an independent predictor.

Virtual gene perturbation analysis

To provide functional evidence beyond statistical association, we performed virtual gene knockout (KO) for E2F7, virtual knockdown (KD) for PBX3 and BCLAF1 (50% expression reduction), and virtual overexpression (OE) for MIF (2-fold overexpression) using GenKI (version 0.2.1), a deep learning

framework that extends the scTenifoldKnk paradigm (single-cell gene regulatory network construction with tensor decomposition and manifold alignment) by replacing linear network comparison with variational graph autoencoders (VGAE) for latent-space perturbation comparison [40], a deep learning framework that predicts gene perturbation effects from single-cell transcriptomic data. Perturbation signatures (|log2FC| > 0.5) were derived for each target gene and cross-referenced with DepMap CRISPR KO screening data [41] and the KnockTF transcription factor perturbation database [42]. Affected pathways were annotated using MSigDB Hallmark gene sets.

Drug sensitivity analysis

We downloaded the drug sensitivity data and gene expression profiles of cancer cell lines from three databases (GDSC1, GDSC2, and Cellminer). First, we selected expression data of head and neck cancer cell lines and calculated Spearman's correlation between the expression of 27 critical TFs and the Area Under the Curve(AUC) of compounds (|cor| > 0.3 and FDR < 0.05). We then analyzed the mechanism of action (MoA) of potential drugs based on CMap results.

Result

The landscape of cell senescence in NPC

In recent years, an increasing number of studies have confirmed that the occurrence and development of tumors are closely related to cell senescence, and changes in cell senescence affect the proliferation, invasion, metastasis, and other biological behaviors of tumor cells. To explore and understand the senescence landscape of NPC cells, we designed CSPCF, a novel framework for classifying cellular senescence status by integrating single-cell transcriptome data and senescence-related gene signatures. Specifically, by screening previous literature, we collected genes related to aging and calculated cell activity scores for each gene signature(Supplementary Table S1). In all seven GMMs, cells assigned to the high (low) senescence score groups were considered high-confidence senescent (normal) cells. These high-confidence cells were used to construct a cellular senescence predictive model based on the XGBoost algorithm.

We applied CSPCF to an NPC dataset (GSE150430), which contains 15 primary NPC tumor samples, and collected clinical information such as pathological classification, clinical stage, and EBV virus infection. The sequencing data were filtered and quality-controlled, and 45,325 cells were annotated as immune cells, malignant cells, or cancer-associated fibroblasts (CAFs) (Fig. 1A). By employing CSPCF, we classified 2710 cells as senescent cells and 34524 cells as normal cells (Fig. 1B). We observed that senescent cells were mainly composed of tumor cells, and the proportion of senescent cells varied among patients with different clinical stages and EBV-infected and non-infected patients (Fig. 1C). Notably, we found that the proportion of senescent cancer cells and senescent immune cells in the microenvironment of EBV-positive NPC tumors is higher, which may be related to the fact that EBV-

encoded latent membrane proteins can trigger cellular senescence through multiple pathways. (Fig. 1D, E).

We screened for differentially expressed genes in cells of different senescence states in the framework. A total of 130 important genes were identified, 47 of which were differentially expressed between senescent and normal tumor cells and immune cells (Fig. 1F). Among these, nine genes, ZWINT, PYCR1, TYMS, and RRM2, were found to be important senescence-related genes. CBS and CDKN2A are differentially expressed only in immune cells. 12 genes as important senescence-related genes were differentially expressed only in tumor cells, such as TOP2A, MCM7, CDC20, CCNB1, etc. Most of these key senescence-related genes have been reported to be involved in various cancer-related processes, for example, overexpression of TPX2 has been reported to be associated with the development of different human tumors and is closely related to chromosomal instability; studies have proved that PYCR1 is highly expressed in a variety of tumors, and it can play a role in promoting tumor growth and proliferation by affecting proline metabolism; FOXM1 has been reported to play an important role in regulating oxidative stress, which contributes to malignant transformation and tumor cell survival.

Exploring the cell-to-cell interactions between immune cells and tumor cells in senescence

The senescence of immune cells, cancer-associated fibroblasts (CAFs), and endothelial cells in the tumor microenvironment (TME) has an important impact on tumor development. As a major component of the tumor immune microenvironment, studies have shown that immune cell senescence leads to immunosuppression and promotes tumor progression. We first explored the senescence landscape of immune cells. We manually annotated immune cells using classical markers, which were identified as B, T, NK, and myeloid cells (Fig. 2A, 2B). Among them, the proportion of senescent B cells was much lower than that of other immune cells (Fig. 2C, 2D). This indicates that B cells have a stronger ability to resist aging in the microenvironment. Next, we divided B cells into senescent B cells (B_senescence) and common B cells (B_Normal) and studied cell-to-cell communication between immune cells and tumor cells by mimicking ligand-receptor interactions. Between various immune cell types and tumor cells, 286 pairs of interactions and eight important signaling pathways were identified (Fig. 2E). By calculating the intensity of the ligand-receptor interactions of selected ligand-receptor pairs in different cell types, we deduced a cell state-specific ligand-receptor interaction network (Fig. 2F). These results indicate that immune cell subtypes display differential susceptibility to senescence in the NPC microenvironment, with B cells exhibiting relative resistance to hypoxia-induced senescence.

For example, tumor cells express relatively high levels of MIF. MIF is a macrophage migration inhibitor that has been reported to promote the proliferation, invasion, and metastasis of tumor cells in a variety of tumors. On the other hand, MIF can also inhibit the apoptosis of tumor cells and enhance their drug resistance, while the corresponding receptors (CD74, CD44) of MIF are widely expressed in senescent cells. This suggests that these ligands play an important role in influencing immune cell infiltration in the senescent microenvironment. Notably, MIF-CD74 interaction had high interaction scores in multiple cell

types (Fig. 2F). We also observed that MIF was predominantly expressed in tumor cells (Fig. 2G), whereas CD74 was predominantly expressed in immune cells (Fig. 2H). Most previous studies have shown that MIF-CD74 signaling prevents macrophage M1 polarization and promotes NPCgenesis. At the same time, senescence not only directly affects macrophage polarization but also promotes tumorigenesis by enhancing peripheral recruitment of myeloid immune cells. Our findings suggest that MIF-CD74 interactions in senescent states play a key role in activating NPC tumor cells to produce a more malignant phenotype. Our findings suggest that MIF-CD74 interactions in the senescent tumor microenvironment play a key role in activating NPC tumor cells to produce a more malignant phenotype and contribute to local immunosuppression.

In addition, we observed significant differences between LGALS9-CD44 and LGALS9-CD45 receptor pairs in senescent and common B cell subsets. LGALS9 (Galectin-9) is a cysteine protein encoded by the Lgals9 gene, which has a specific domain and is widely present in immune cells and certain tumor cells. It plays an important role in immune regulation and tumor development, regulating T-cell differentiation and function by interacting with other molecules, promoting antiviral and antitumor immune responses, and inhibiting inflammatory responses. In addition, LGALS9 is involved in the growth and metastasis of tumors, affecting the proliferation, migration, and invasion ability of cells. LGALS9 and its receptors, CD44 and CD45, were highly expressed in senescent B cells (Fig. 2F). Together, these results establish that multiple ligand-receptor axes, including MIF-CD74 and LGALS9-CD44/CD45, mediate communication between senescent tumor cells and the surrounding immune microenvironment in NPC, with implications for immune evasion.

Deciphering heterogeneity of the senescence state and function of NPC tumor cells. To explore the heterogeneity of tumor cell senescence status in NPC, we first divided 8021 tumor cells into 1663 (20.73%) senescent cells and 6358 (79.17%) common cells by CSPCF and performed cluster analysis on common and senescent tumor cells, respectively, and identified five hypoxic subpopulation subsets (S1, S2, S3, S4, S5; Fig. 3A) and six common subpopulations (named N1, N2, N3, N4, N5, and N6; Fig. 3B). The "senescence score" of each tumor cell was calculated based on the expression of 20 important senescence genes (Fig. 3C). We found that the senescence scores of the N1, N2, N3, N4, N5, and N6 subsets were significantly lower than those of the S1, S2, S3, and S4, S5 subsets, and the S2 subsets had the highest aging scores compared with the other subgroups in all subsets (Fig. 3C). Figure 4D illustrates the unique expression of genes in each subpopulation. Interestingly, marker genes in the high-aging score subset have previously been shown to be associated with tumor progression, for example, Cell division cycle-associated protein 2 (CDCA2) and transmembrane protein 35(TMEM35). CDCA2 is an important member of the cell division cycle-associated (CDCA) gene family, an important regulator of cell proliferation, and is involved in chromatin remodeling during mitosis, the DNA damage response in the cell cycle, and nuclear envelope formation. Recent studies have confirmed that CDCA2 is upregulated in a variety of tumors, including breast cancer and oral squamous cell carcinoma. As a member of the transmembrane protein gene family, TMEM35 is widely involved in the composition of cell membrane structures, such as the endoplasmic reticulum, lysosomes, and Golgi apparatus, and has been associated with the proliferation, invasion, and migration of cancer cells, as well as chemotherapy

resistance (Fig. 3D). GO functional enrichment revealed that the genes of the high-aging scoring subsets were concentrated in the DNA mitotic cell cycle and the regulation of primary metabolic process pathways (Fig. 3E). Together, these results demonstrate that senescent NPC tumor cells are transcriptionally heterogeneous and segregate into subpopulations with distinct gene expression programs.

We employed high-dimensional weighted gene co-expression network analysis to identify the key gene modules for each subpopulation. After setting the soft threshold to 6, we obtained 17 gene modules. Interestingly, the magenta module showed abundant expression in the S2 cell subset, while the red modules were highly expressed in the N4 cell subset, and the pink modules were highly expressed in the N3 cell subset (Fig. 3F). We also calculated the odds ratio of the overlap of the differential genes among the eight cell subpopulations of N1, N2, N3, N4, N5, N6, S1, S2, S3, S4, and S5 with the key genes of each module, and the results further suggested that the magenta module enrichment genes had a high overlap with the differentially expressed genes of the S2 subpopulation, (odds ratio (OR) = 14.14372754), while the red module enrichment genes were highly overlapped with the characteristic genes of the N4 subset ((OR) = 5.21660823), pink module enrichment genes were highly overlapped with the characteristic genes of the N3 subset ((OR) = 17.76443497) (Fig. 3G). Through KEGG enrichment analysis, we found that the key genes of the magenta module were enriched in the cell cycle, DNA replication, and mismatch repair pathways, while the key genes of the pink module were enriched in the Toll-like receptor signaling pathway, endocytosis, apoptosis, and T cell receptor signaling pathway(Fig. 3H, 3I). It is worth noting that most of the pathways enriched in the pink and red modules are related to immune and inflammatory signals, whereas most of the pathways enriched in the magenta module have been confirmed to affect genome stability. In addition, CytoTRACE was used to calculate the differentiation status of each tumor subset and explore the correlation between senescence status and cell differentiation. These analyses link the S2-specific magenta module to cell cycle dysregulation, DNA replication stress, and mismatch repair deficiency, providing functional annotation of the senescence-associated transcriptional program.

We found that the S1 and S2 subpopulations had higher differentiation scores and the N3 and N4 subsets had lower differentiation scores (Fig. 3J). Subsequent trajectory analysis revealed that tumor cells with high senescence scores (S2 subpopulation) were at the end of the pseudo-temporal trajectory, and tumor cells with low senescence scores (N4 subpopulation) were at the beginning of the pseudo-temporal trajectory (Fig. 3k). Combined with the results of the GO functional enrichment analysis, we speculate that the trajectory of tumor cell differentiation is accompanied by a transformation of aging characteristics, which can be manifested as a change from a state of uncontrolled cell cycle dominated by DNA damage and genomic instability to a state of inflammatory pathway activation dominated by cytokine production and T cell differentiation. Overall, pseudotemporal trajectory analysis positions the S2 subpopulation at the terminal end of tumor cell differentiation, suggesting that senescence represents a functional endpoint of NPC tumor cell evolution associated with genomic instability and proliferative arrest.

Develop comprehensive cell state-specific gene regulatory networks and identify key regulators associated with senescence-mediated tumor invasion in the early phases of tumor cell neoplastic differentiation.

In the functional analysis, we found that NPC tumor cells had a higher senescence score in the early stages of differentiation and were closely related to the genomic instability of tumor cells, which is closely associated with tumor progression and chemotherapy resistance. Therefore, we further explored the association between the senescence score in NPC and the characteristics of tumor progression and chemotherapy resistance. We obtained 14 sets of tumor characteristic genes related to tumor differentiation, tumor proliferation, tumor metastasis, angiogenesis, EMT and Platinum resistance from the Cancer SEA database, extracted 10 from the literature, and a set of typical cancer marker genes for different types of cancer (reference: PMCID: PMC8526411, PMID: 40148533). The activity score of each cell subpopulation for each cell was calculated using GSVA. The results indicated that tumor proliferation, cell cycle, and immune destruction avoidance were significantly positively correlated with the senescence score (Fig. 4A). Overall, our results emphasize that the S2 subpopulation of cells represents an aging phenotype with high proliferation potential and immune evasion ability. To further clarify the tumor-specific regulatory mechanisms of tumor cells with high senescence scores, SCENIC was used to construct cell state-specific gene regulatory networks (GRNs) in the S2 and N4 subpopulations. We then used the centrality metrics of the network (including betweenness centrality, PageRank, Degree centrality, and closeness centrality) to identify the key genes in each GRN. The Q statistic was used to integrate the four central indicators, and the genes ranked in the top 1% by the Q statistic were regarded as key genes (Fig. 4B). A total of 39 and 29 key transcription factors were identified in the S2 and N4 subgroups, respectively. Among the 39 transcription factors in the S2 subgroup, 33 were specific to this S2 subgroup (Fig. 4C). They are believed to play an important regulatory role in the invasion of tumor cells with high senescence scores.

Next, we conducted GSVA based on the MSigDB marker gene set to evaluate the cancer-related pathways involved in 33 TFs and their target genes (regulators). Most of these TFs and their target genes were positively correlated with hypoxia, EMT, apoptosis, P53, and KRAS pathways, especially E2F2, E2F7, and E2F8 (Fig. 4D). E2F2, E2F7, and E2F8 are important members of the E2F transcription factor family. The E2F transcription factor family is involved in the occurrence and progression of various tumors by influencing processes such as cell proliferation, cell death, DNA damage response, dryness, epithelial-mesenchymal transition, metastasis, and chemotherapy resistance. E2Fs have been reported to be elevated in various human malignant tumors, such as colorectal, esophageal, head and neck, kidney, lung adenocarcinoma, breast, liver, colorectal, gastric, and bladder cancers, and are associated with poor prognosis and treatment resistance. E2F2 and E2F7 have been reported to interact with factors such as PTPRD, p53, OCT1, let-7a, and B-Myb and are involved in pathways such as Wnt/β-catenin, PTEN/AKT, and PI3K/AKT. Studies have shown that E2F8 knockdown makes breast cancer cells sensitive to azolicin and cisplatin.

Key TFs associated with high senescence states can predict clinical outcomes.

To determine whether 33 key TFs contribute to clinical treatment and guide the prognosis of NPC, we performed a survival analysis using a cohort of 97 patients from the GEO head and neck cancer dataset GSE41613 as the training set. We focused on three TFs associated with OS using univariate Cox proportional hazards regression (log-rank test, $p < 0.05$). Subsequently, stepwise regression analysis was used to further screen genes associated with OS and three TFs (PBX3, FOXP1, and BCLAF1; Fig. 5A) to construct the final prognostic model. We calculated the risk score for each patient based on the expression levels of the three TFs weighted by the regression coefficients in univariate Cox proportional hazards regression analysis. We divided the patients into high-($n = 48$) and low-risk ($n = 49$) groups based on the median risk score. KM curves showed that the OS was significantly shorter in the high-risk group than in the low-risk group (log-rank test, $p < 0.001$; Fig. 5B). Multivariate Cox regression analysis was conducted to assess whether the three-gene signature was an independent prognostic factor. Covariates included age, sex, and stage. The results showed that our three-gene signature could independently predict poorer OS in patients (HR = 0.42 [0.18–0.99], $P < 0.05$) (Fig. 5C). Finally, we validated the prognostic value of the three-gene signature in an external validation dataset (GSE65858), in which the KM curve differences between the two groups were significant ($p = 0.046$, Fig. 5D). The modest significance in the external validation cohort likely reflects limited sample size and biological differences between NPC and other head and neck cancers, warranting further validation in a dedicated NPC cohort. While the 3-TF model demonstrates promising discriminative ability, validation in larger NPC-specific cohorts with complete clinical annotation is warranted to confirm its clinical utility.

Potential targeted therapeutic drugs for senescence - related targets

To characterize the therapeutic significance of 33 key TFs in clinical applications, we integrated four large-scale drug sensitivity datasets (CellMiner, GDSC1, GDSC2, CTRPV2). The correlation between the expression levels of these 33 key TFs and the half-maximal inhibitory concentration (IC50) of chemotherapy drugs in the CellMiner, GDSC1, and GDSC2 databases was calculated. In the CTRP database, we calculated the associations between the expression of 33 TFs and the area under the curve (AUC) of drugs. Screening was conducted when $R > 0.3$ when $P < 0.05$, screening was conducted. Finally, the intersection of the compounds screened from the four databases was used to obtain six key compounds ($cor > 0.3$, $p < 0.05$, Fig. 6A-E).

Virtual gene perturbation validates functional roles of key senescence-associated TFs

To strengthen the causal evidence beyond statistical associations, we performed in silico gene perturbation analysis using GenKI. Virtual KO of E2F7 predicted downregulation of cell cycle drivers (MKI67, CCNE1, CCNB1, CDC25A) and upregulation of apoptosis-related genes (GADD45A, BBC3, TP53INP1, BAX), consistent with reversal of the proliferative senescence phenotype (Fig. 7A). PBX3 virtual KD attenuated EMT-associated genes (SNAI1, MMP2, HOXA9) while upregulating epithelial

markers (CDH1, EPCAM) (Fig. 7B). BCLAF1 KD impaired DNA repair through downregulation of RAD51, BRCA1, and TP53BP1, with compensatory upregulation of pro-apoptotic effectors (BAX, BAK1, CASP3), suggesting synthetic lethality potential with DNA-damaging agents (Fig. 7C). MIF overexpression enhanced expression of pro-inflammatory cytokines (TNF, IL6, CXCL8, VEGFA) and upregulation of CD74, coupled with suppression of anti-tumor immune effectors (IL10, TGFB1, IFNG), indicating M2 macrophage polarization and establishment of an immunosuppressive TME (Fig. 7D). These virtual perturbation results provide in silico functional validation bridging correlative findings to causal regulatory roles of key genes in NPC senescence-driven immunosuppression. Notably, the co-occurrence of multiple E2F family members within the same senescent subpopulation suggests a dysregulated cell cycle state wherein proliferative and senescence-associated programs coexist — a phenomenon implicated in therapy resistance across several solid tumor types. Future functional studies will be required to dissect the individual versus cooperative roles of these E2F factors in NPC senescence. While other prognostic biomarkers have been proposed for NPC, including GNA14 [29], the senescence-associated TF signature identified here captures a unique axis linking tumor hypoxia to immune evasion.

Discussion

Our study provides a comprehensive single-cell dissection of the hypoxic microenvironment in NPC, establishing a robust link between cellular hypoxia, immune senescence, and tumor invasion [19–22]. By developing and applying the CSPCF framework, we identified a distinct hypoxic subpopulation (S2), characterized by high senescence scores, elevated proliferative potential, and immune evasion capabilities. This subpopulation is driven by a specific set of transcription factors, including key E2F family members (E2F2, E2F7, and E2F8), which coordinate protumorigenic pathways related to the cell cycle, DNA replication, and hypoxia response [23, 24]. The central finding of our study is the identification of the MIF-CD74 ligand-receptor pair as a critical mediator of cellular crosstalk within the senescent microenvironment, contributing to an immunosuppressive niche that facilitates tumor progression and may underlie radioresistance [25–27]. Preclinical evidence indicates that pharmacological blockade of MIF-CD74 signaling can restore antitumor immune responses [35], and MIF-targeted therapeutic strategies are under active investigation [36]. Our single-cell findings align with recent high-resolution transcriptomic studies of NPC that have characterized the tumor immune microenvironment [37–39]. The ability to predict perturbation signatures from unperturbed single-cell transcriptomes provides a complementary approach to traditional in vitro experiments, particularly for transcription factors whose knockout is technically challenging. Cross-referencing with DepMap CRISPR screening [41] and KnockTF perturbation data [42] provided orthogonal support for the functional predictions. Collectively, these data support a model wherein hypoxia- and EBV-driven senescence establishes an immunosuppressive niche via MIF-CD74 and LGALS9 axes, facilitating tumor immune evasion and therapy resistance.

A key innovation of this study lies in the CSPCF framework, which enabled high-confidence classification of senescence states from scRNA-seq data. This approach revealed that senescence is not a uniform state, but exhibits significant heterogeneity, with the S2 subpopulation being particularly enriched in malignant cells. The strong association between the senescence score and processes such as

Avoiding_Immune_Destruction suggests that senescent tumor cells may actively remodel the immune landscape. This is further supported by our cell-cell communication analysis, which pinpoints the MIF-CD74 axis. Although MIF is known to be involved in tumorigenesis, our data specifically implicate its role in hypoxia-induced senescence in NPC. The expression pattern of MIF in tumor cells and its receptor CD74 on immune cells suggest a paracrine mechanism in which tumor cells modulate immune function. This finding aligns with prior studies showing that MIF-CD74 signaling promotes a tumor-permissive environment [13, 16], and we extended this by linking it to the senescent hypoxic niche in NPC.

The 33 S2-specific TFs, particularly E2F factors, represent a novel regulatory hub. E2Fs are well-established drivers of cell proliferation, but their connection to a senescence-associated, hypoxic invasive phenotype in NPC has been less explored. Our GSVA results indicated that the activity of these TFs is correlated with hypoxia, EMT, and apoptosis pathways, positioning them as central regulators of the aggressive traits observed in the S2 subpopulation. The prognostic model built on three of these TFs (PBX3, FOXP1, and BCLAF1) demonstrated significant predictive power in independent cohorts, underscoring their clinical relevance [28]. This model effectively stratified patients into distinct risk groups, with the high-risk group showing a strong association with poorer overall survival independent of conventional clinical variables.

A potential limitation of this study was its reliance on transcriptional data from bulk and single-cell sequencing. Although we inferred critical regulatory networks and cell-cell interactions, functional validation using in vitro and in vivo models is required to definitively establish causality. Future studies should focus on experimentally disrupting key nodes, such as MIF-CD74 signaling or individual E2F factors, to confirm their roles in invasion and therapy resistance [29, 30]. Furthermore, the therapeutic vulnerabilities identified through drug sensitivity analysis, although promising, require empirical testing in preclinical models of NPC [31–34]. Second, the independent validation cohort (GSE65858) comprised head and neck cancers, not NPC exclusively, warranting further validation in a dedicated NPC cohort. Third, the scRNA-seq dataset included only one normal tissue sample, limiting the statistical power of tumor-versus-normal comparisons.

Virtual gene perturbation analysis provided in silico functional validation of the key senescence-associated TFs identified in this study. Virtual KO of E2F7 predicted reversal of the proliferative senescence phenotype through cell cycle arrest and apoptosis activation, while PBX3 KD attenuated EMT-associated invasion programs and BCLAF1 KD impaired DNA repair, suggesting synthetic lethality potential with DNA-damaging agents. MIF overexpression enhanced the expression of pro-inflammatory cytokines and CD74, confirming its central role in shaping the immunosuppressive TME via the MIF-CD74 axis. These in silico predictions, cross-referenced with DepMap CRISPR screening data, provide a roadmap for prioritizing these targets for experimental validation.

In conclusion, our work moves beyond correlative analysis to propose a mechanistic model wherein hypoxia fosters a senescent tumor subpopulation that leverages specific TF networks and the MIF-CD74 axis to drive invasion and immune suppression. The defined three-gene signature offers a tangible tool

for prognostic stratification, and the identified ligand-receptor pair and key TFs present new avenues for developing targeted therapies aimed at disrupting the hypoxic, senescent niche to improve outcomes in NPC patients. Future studies should prioritize functional validation of MIF-CD74 blockade in NPC models, prospective assessment of the 3-TF signature in NPC cohorts, and investigation of whether EBV-encoded latent proteins directly induce senescence programs, which would establish a mechanistic link between the defining viral etiology of NPC and the immunosuppressive senescence phenotype identified herein.

Declarations

- **Ethical Approval** Not Applicable.
- **Consent to Participate** Not Applicable.
- **Consent to Publish** Not Applicable.

Funding None.

Competing Interests The authors declare no competing interests

Author Contributions Taoyuan Xiao: Conceptualization, Data curation, Formal analysis, Methodology, Software, Visualization, Writing – original draft. Ying Zhang: Data curation, Formal analysis, Investigation, Writing – review & editing. Quan Li: Formal analysis, Validation, Writing – review & editing. Xianfang Chen: Investigation, Resources, Writing – review & editing. Fusen Peng: Conceptualization, Project administration, Supervision, Writing review & editing. All authors reviewed the manuscript.

Data Availability The single-cell RNA sequencing dataset analyzed in this study is publicly available from the NCBI Gene Expression Omnibus (GEO) database[https://www.ncbi.nlm.nih.gov/geo/query/acc.cgi?acc=GSE150430] under accession number GSE150430. The bulk RNA-seq datasets are available from GEO under accession numbers GSE65858 [https://www.ncbi.nlm.nih.gov/geo/query/acc.cgi?acc=GSE65858] and GSE41613 https://www.ncbi.nlm.nih.gov/geo/query/acc.cgi?acc=GSE41613]. The senescence gene sets were obtained from the Molecular Signatures Database (MSigDB) [https://www.gsea-msigdb.org/gsea/msigdb/]. Drug sensitivity data were downloaded from the Genomics of Drug Sensitivity in Cancer (GDSC) database [https://www.cancerrxgene.org/] and the CellMiner database [https://discover.nci.nih.gov/cellminer/]. All data generated or analyzed during this study are included in this published article and its supplementary information files.

References

1. Chen YP, Chan ATC, Le QT, Blanchard P, Sun Y, Ma J. Nasopharyngeal carcinoma. Lancet. 2019;394:64–80. https://doi.org/10.1016/S0140-6736(19)30956-0.
2. Wong KCW, Hui EP, Lo KW, et al. Nasopharyngeal carcinoma: an evolving paradigm. Nat Rev Clin Oncol. 2021;18:679–95. https://doi.org/10.1038/s41571-021-00524-x.

3. Zhang Y, Wu T, Miao W, et al. Global, regional, and national burden of nasopharyngeal carcinoma from 1990 to 2021. Laryngoscope. 2024;134:5035–44. https://doi.org/10.1002/lary.31623.
4. Peng G, Cao S, Chen J. Advances in single-cell sequencing technology and its application in tumor research. Cell Res. 2023;33:731–46. https://doi.org/10.1038/s41422-023-00852-8.
5. Blanchard P, Lee AWM, Leclercq G, et al. Meta-analysis of chemotherapy in nasopharyngeal carcinoma (MAC-NPC). Lancet Oncol. 2023;24:609–22. https://doi.org/10.1016/S1470-2045(23)00189-4.
6. Zhang MX, Li J, Shen GP, et al. Intensity-modulated radiotherapy prolongs survival of nasopharyngeal carcinoma patients. Cancer. 2024;130:834–42. https://doi.org/10.1002/cncr.35082.
7. You R, Liu YP, Huang PY, et al. Efficacy and safety of PD-1/PD-L1 inhibitors in recurrent or metastatic NPC: a meta-analysis. Oral Oncol. 2023;145:106534. https://doi.org/10.1016/j.oraloncology.2023.106534.
8. Lee AWM, Ng WT, Chan JYW, et al. Management of locally recurrent nasopharyngeal carcinoma. Cancer Treat Rev. 2019;79:101890. https://doi.org/10.1016/j.ctrv.2019.101890.
9. Li Y, Hong X, Xu W, et al. Radiosensitivity-related gene prognostic model in nasopharyngeal carcinoma. Transl Oncol. 2024;42:101896. https://doi.org/10.1016/j.tranon.2024.101896.
10. Huang X, Lin K, Chen W, et al. Local angiotensin II modulation augments ferroptosis and radiosensitivity in NPC via AT1R blockade. Theranostics. 2024;14:3321–38. https://doi.org/10.7150/thno.95762.
11. Lan Y, Zhao S, Hou T, Ren Y. Mechanism of HIF-1α promoting proliferation, invasion and metastasis of NPC by regulating MMP-2. J Cell Mol Med. 2021;25:7942–53. https://doi.org/10.1111/jcmm.16721.
12. Suvac A, Ashton J, Bristow RG. Tumour hypoxia in driving genomic instability and tumour evolution. Nat Rev Cancer. 2025;25:167–88. https://doi.org/10.1038/s41568-024-00781-9.
13. Chen Z, Han F, Du Y, Shi H, Zhou W. Hypoxic microenvironment in cancer: molecular mechanisms. Signal Transduct Target Ther. 2023;8:70. https://doi.org/10.1038/s41392-023-01332-8.
14. Yang Z, Su W, Wei X, et al. HIF-1α drives cancer resistance to cuproptosis. Cancer Cell. 2025;43:398–415. https://doi.org/10.1016/j.ccell.2025.02.015.
15. Muz B, de la Puente P, Azab F, Azab AK. The role of hypoxia in cancer progression. Hypoxia. 2015;3:83–92. https://doi.org/10.2147/HP.S93413.
16. Harris AL. Hypoxia—a key regulatory factor in tumour growth. Nat Rev Cancer. 2002;2:38–47. https://doi.org/10.1038/nrc704.
17. Zhang Y, Zhang B, Lv C, et al. scRNA-seq identifies critical TFs of tumor cell invasion induced by hypoxia in glioblastoma. Theranostics. 2023;13:2189–205. https://doi.org/10.7150/thno.82234.
18. Fane M, Weeraratna AT. How the ageing microenvironment influences tumour progression. Nat Rev Cancer. 2020;20:89–106. https://doi.org/10.1038/s41568-019-0222-9.

19. Zhao B, Wu B, Feng N, et al. Aging microenvironment and antitumor immunity. J Hematol Oncol. 2023;16:28. https://doi.org/10.1186/s13045-023-01426-4.
20. Sattiraju A, Kang S, Giotti B, et al. Hypoxic niches attract and reprogram TAMs and CTLs for immunosuppression. Immunity. 2023;56:1825–e18436. https://doi.org/10.1016/j.immuni.2023.06.017.
21. Terroba-Navajas P, Lu IN, Quast I, et al. scRNA-seq identifies MIF-CD74 axis in myasthenia gravis thymus. Neurol Neuroimmunol Neuroinflamm. 2025;12:e200381. https://doi.org/10.1212/NXI.0000000000200381.
22. Kent LN, Leone G. The broken cycle: E2F dysfunction in cancer. Nat Rev Cancer. 2019;19:326–38. https://doi.org/10.1038/s41568-019-0143-7.
23. Sun M, Ji Y, Zhang G, et al. Posttranslational modifications of E2F family members. Biomed Pharmacother. 2024;172:116251. https://doi.org/10.1016/j.biopha.2024.116251.
24. Inayatullah M, Mahesh A, Turnbull AK, et al. Basal-epithelial subpopulations predict chemotherapy resistance in TNBC. EMBO Mol Med. 2024;16:294–318. https://doi.org/10.1038/s44321-023-00020-6.
25. Ngernsombat C, Suriya U, Prattapong P. Repurposing FDA-approved drugs targeting FZD10 in NPC. Sci Rep. 2024;14:15678. https://doi.org/10.1038/s41598-024-66701-x.
26. Zhao Y, Li J, Dian M. N6-methyladenosine methylation in nasopharyngeal carcinoma. Cell Death Discov. 2024;10:89. https://doi.org/10.1038/s41420-024-01845-3.
27. Li H, Lou L, Du J, et al. Multimodal profiling uncovers tertiary lymphoid structures in NPC. Cancer Cell. 2024;42:1452–67. https://doi.org/10.1016/j.ccell.2024.07.008.
28. Zhang Y, Zou Q, Zhao B, et al. Toripalimab plus anlotinib in recurrent or metastatic NPC. Nat Med. 2024;30:2890–8. https://doi.org/10.1038/s41591-024-03211-7.
29. Hao J, Yu X, Xiong L, et al. GNA14 as a potential prognostic biomarker in NPC. Front Oncol. 2024;14:1387654. https://doi.org/10.3389/fonc.2024.1387654.
30. Lánczky A, Győrffy B. Web-based survival analysis tool (KMplot). J Med Internet Res. 2021;23:e27633. https://doi.org/10.2196/27633.
31. Jin S, Guerrero-Juarez CF, Zhang L, et al. Inference and analysis of cell-cell communication using CellChat. Nat Commun. 2021;12:1088. https://doi.org/10.1038/s41467-021-21246-9.
32. Aibar S, González-Blas CB, Moerman T, et al. SCENIC: single-cell regulatory network inference. Nat Methods. 2017;14:1083–6. https://doi.org/10.1038/nmeth.4463.
33. Hänzelmann S, Castelo R, Guinney J. GSVA: gene set variation analysis. BMC Bioinformatics. 2013;14:7. https://doi.org/10.1186/1471-2105-14-7.
34. Subramanian A, Tamayo P, Mootha VK, et al. GSEA: a knowledge-based approach for interpreting genome-wide expression profiles. Proc Natl Acad Sci USA. 2005;102:15545–50. https://doi.org/10.1073/pnas.0506580102.

35. Figueiredo CR, Azevedo RA, Mousdell S, et al. Blockade of MIF-CD74 signalling restores antitumour immune response. Front Immunol. 2018;9:1132. https://doi.org/10.3389/fimmu.2018.01132.
36. Bucala R. MIF, MIF alleles, and prospects for therapeutic intervention. J Clin Immunol. 2013;33(Suppl 1):S72–8. https://doi.org/10.1007/s10875-012-9781-1.
37. Chen YP, Yin JH, Li WF, et al. scRNA-seq reveals regulators of immune cell diversity in NPC. Cell Res. 2020;30:1024–42. https://doi.org/10.1038/s41422-020-0374-x.
38. Liu Y, He S, Wang XL, et al. Tumour heterogeneity of NPC at single cell resolution. Nat Commun. 2021;12:741. https://doi.org/10.1038/s41467-021-20943-1.
39. Gong L, Kwong DLW, Dai W, et al. Comprehensive scRNA-seq of NPC microenvironment. Nat Commun. 2021;12:1540. https://doi.org/10.1038/s41467-021-21721-9.
40. Yang Y, Li G, Zhong Y, et al. GenKI: predicting gene knockout effects from single-cell transcriptomes. Nucleic Acids Res. 2023;51:W384–92. https://doi.org/10.1093/nar/gkad450.
41. Tsherniak A, Vazquez F, Montgomery PG, et al. Defining a cancer dependency map. Cell. 2017;170:564–e57616. https://doi.org/10.1016/j.cell.2017.06.010.
42. Feng C, Song C, Liu Y, et al. KnockTF: gene expression profile database for gene perturbation. Nucleic Acids Res. 2023;51:D1237–44. https://doi.org/10.1093/nar/gkac965.

Figures

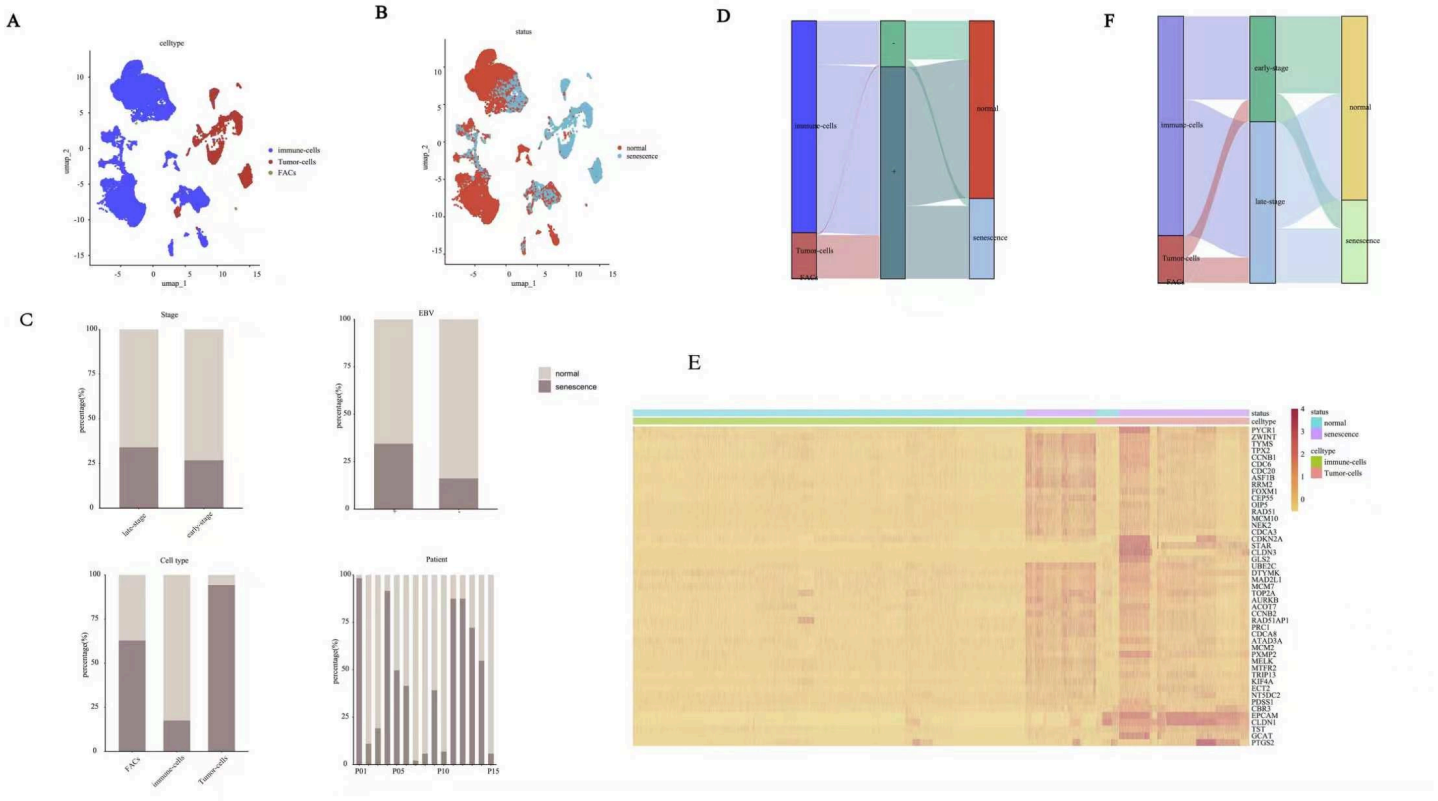


Figure 1

Single-cell landscape and identification of senescent cells in NPC. (A) UMAP visualization of all single cells colored by their predicted state: normal cells (blue) and senescent cells (red). (B) Proportion of senescent cells in each cell type. (C) Distribution of senescent cells by clinical stage and EBV infection status. (D, E) Senescent cell proportion in EBV-positive vs. EBV-negative NPC tumors. (F) Heatmap of differentially expressed genes between senescent and normal cells.

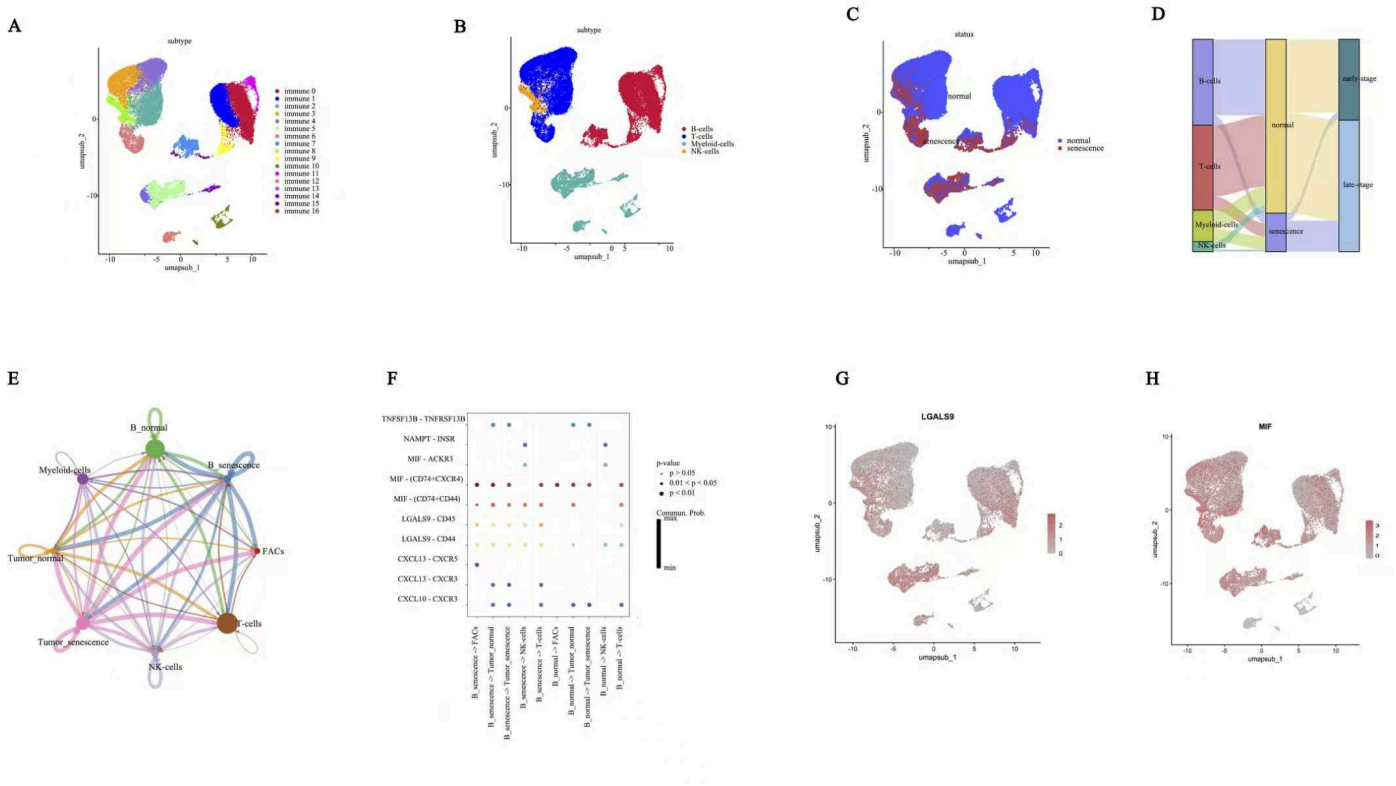


Figure 2

Cellular communication and immune landscape.(A, B) UMAP of immune cell subtypes and their senescence proportions. (C, D) Senescent cell distribution across B, T, NK, and myeloid cells. (E) CellChat ligand-receptor interaction network between immune and tumor cells. (F) Ligand-receptor interaction heatmap showing MIF-CD74 as the top interaction axis. (G) Feature plot of MIF expression. (H) Feature plot of CD74 expression.

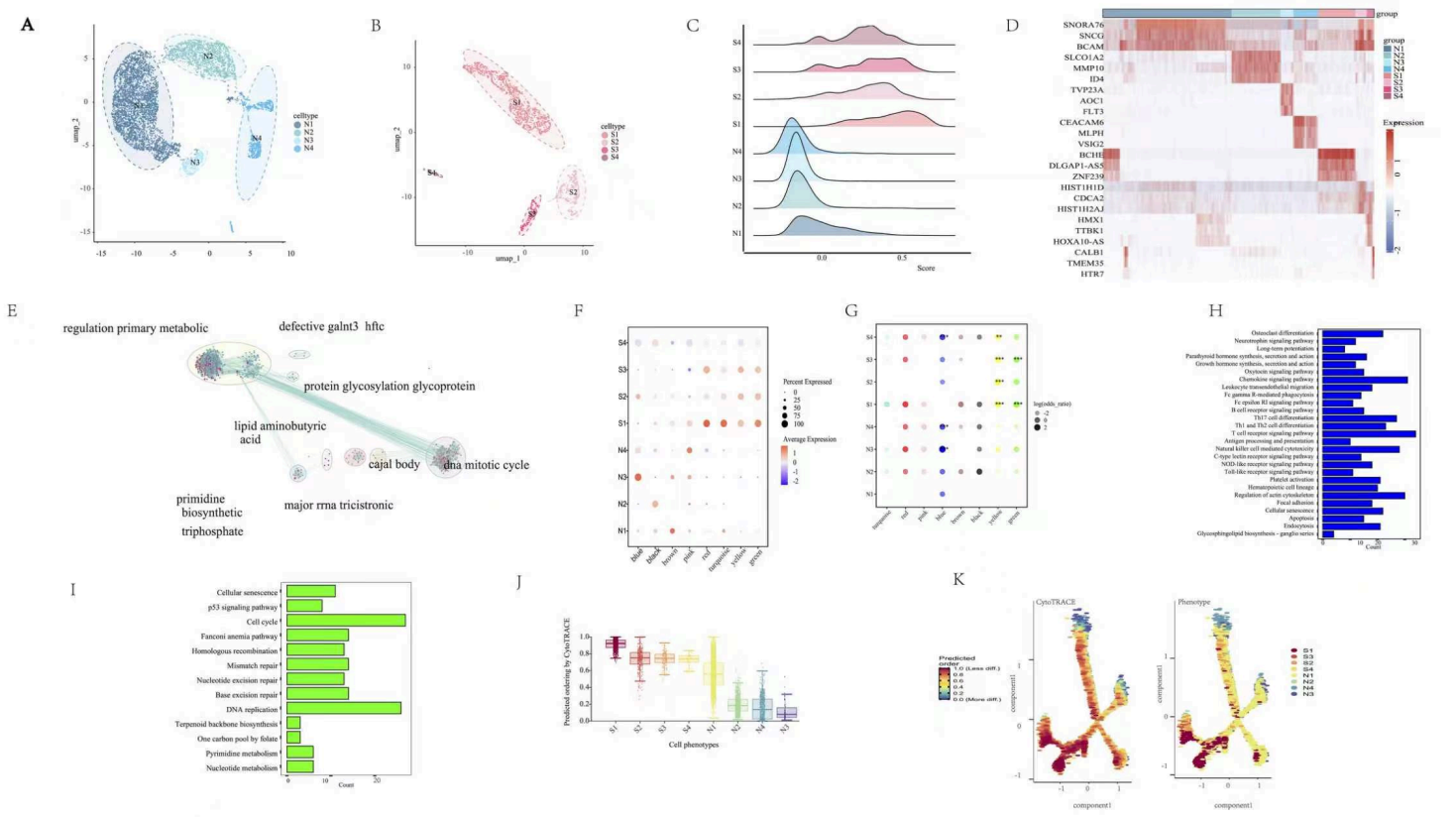


Figure 3

Cellular composition and tumor cell subpopulation analysis. (A) UMAP projection of all cells colored by their origin: normal (blue) and tumor (red). (B) t-SNE clustering of tumor cells identifying distinct transcriptional subpopulations. (C) Cell-type proportions across senescence states. (D) Expression heatmap of marker genes for each tumor subpopulation. (E) Feature plots of key senescence markers. (F) Subpopulation distribution by clinical stage. (G) Cell cycle phase distribution. (H) SCENIC regulatory network for S2-specific TFs. (I) E2F family expression across subpopulations. (J) Differentially expressed genes between S1 and S2 subpopulations. (K) Senescence score density by subpopulation.

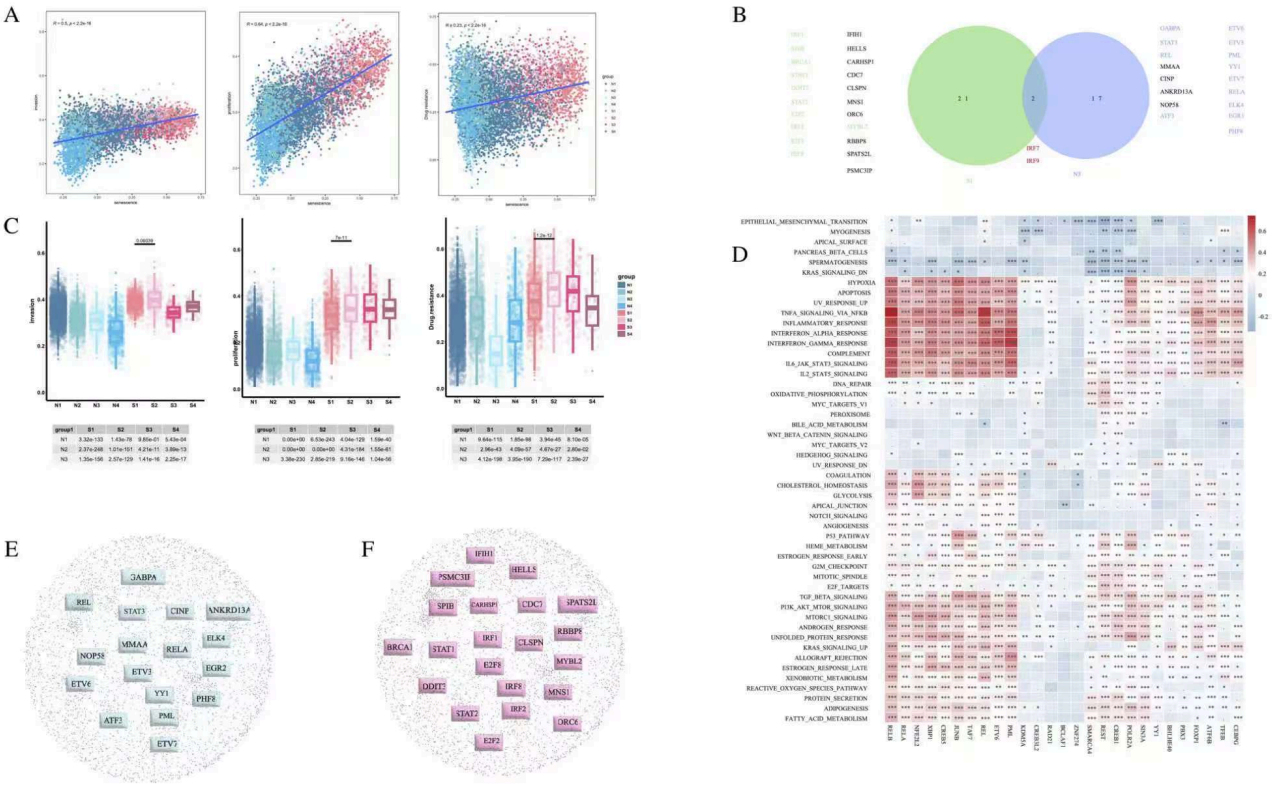


Figure 4

Functional enrichment and pathway activity in distinct cell states. (A) Heatmap of GSVA scores showing correlations between senescence scores and cancer hallmark pathway activities. (B) Bubble plot of GO enrichment analysis for S2-specific genes. (C) GSEA plots showing enrichment of EMT, hypoxia, and cell cycle pathways. (D) KEGG pathway enrichment network. (E) Transcription factor activity across cell states. (F) Pathway-level comparison between S1 and S2 subpopulations.

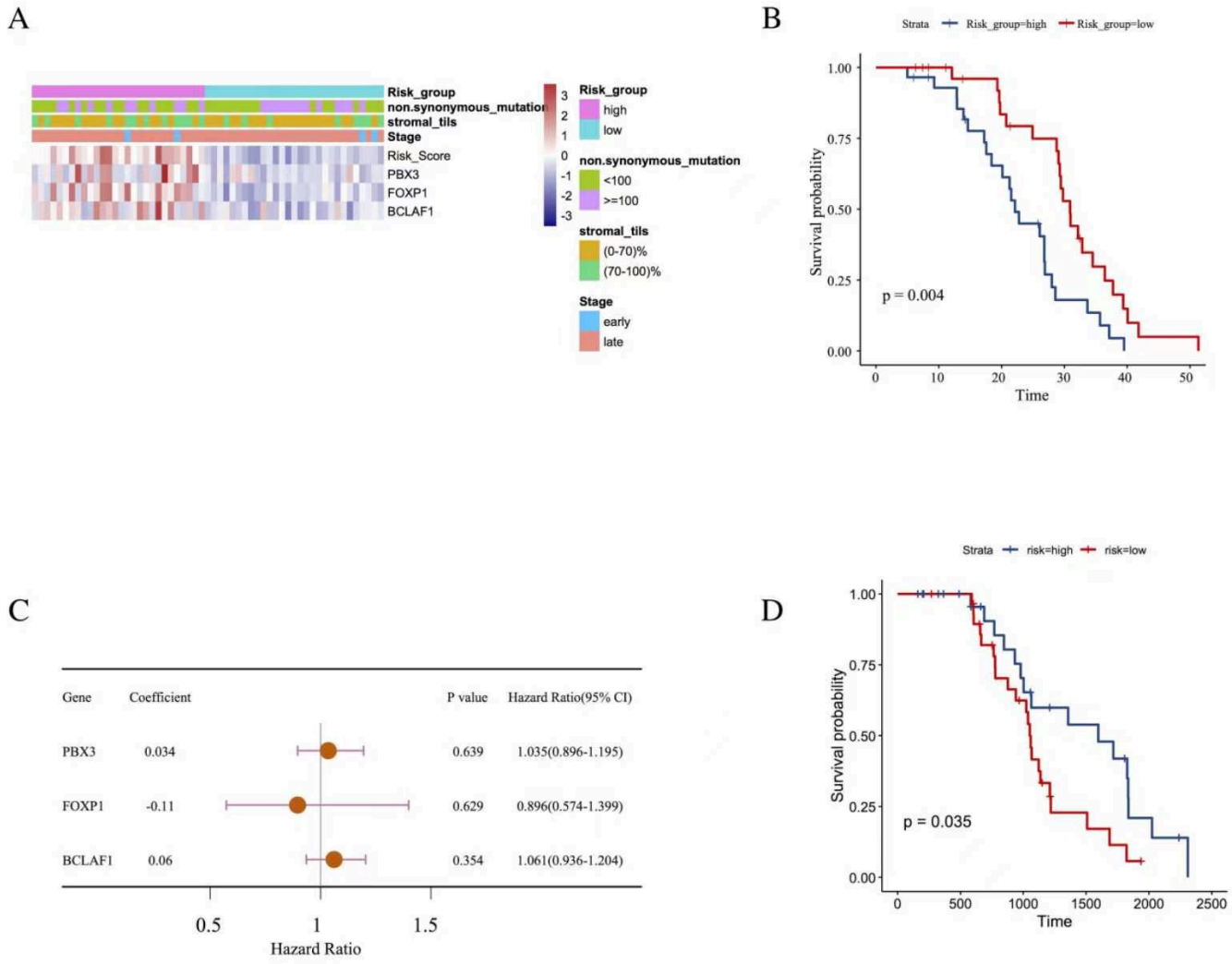


Figure 5

Gene Set Enrichment Analysis (GSEA) of signature pathways. (A) Forest plot of univariate Cox regression analysis for 33 key TFs in the training cohort (GSE41613, n=58). (B) Kaplan-Meier survival curves for the 3-TF prognostic model in the training cohort. (C) KM curves in the independent validation cohort. (D) Multivariate Cox regression results showing the risk score as an independent prognostic factor. (E) Time-dependent ROC curves at 1, 3, and 5 years. (F) Risk score distribution and survival status by patient.

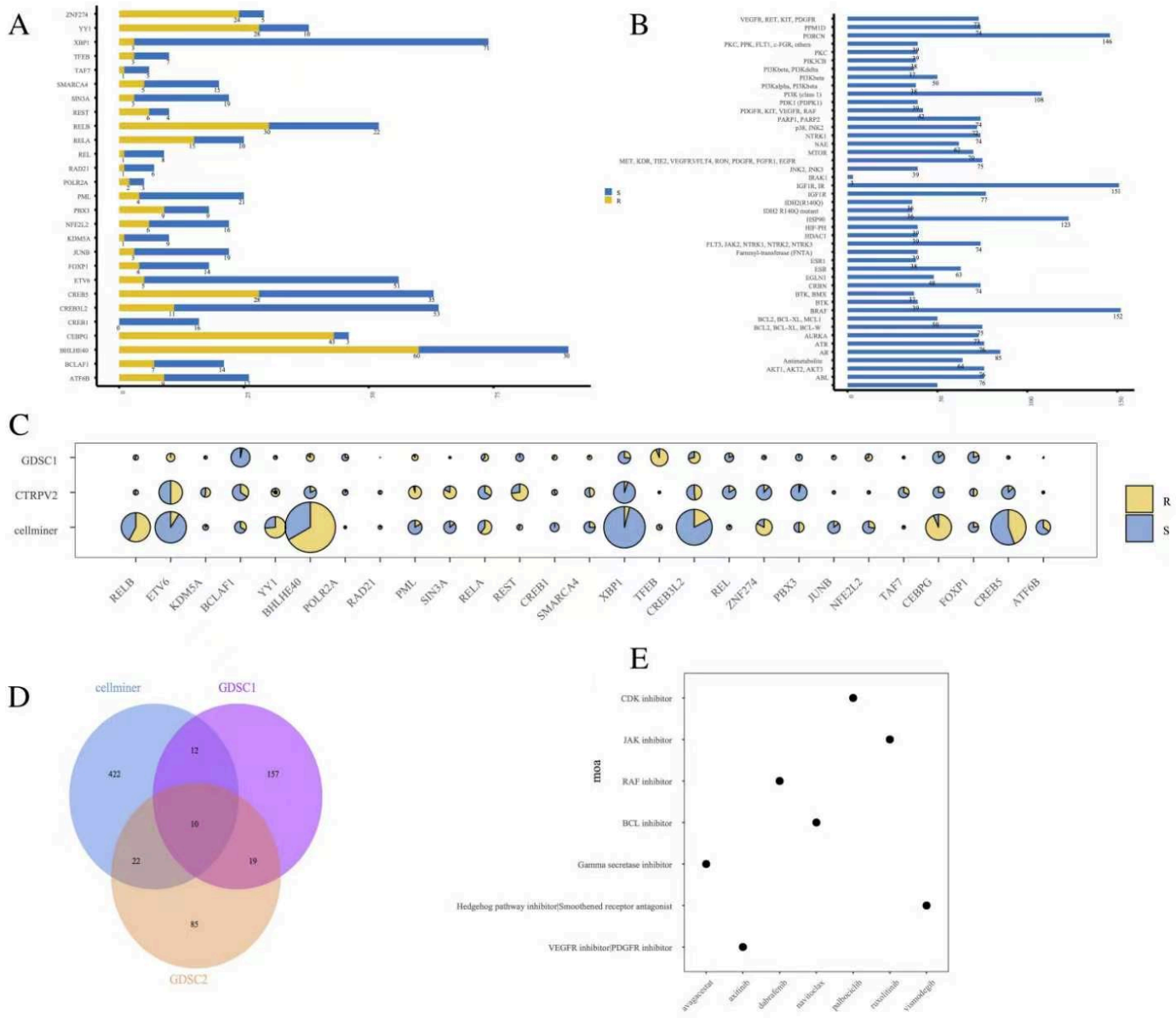


Figure 6

Prognostic validation of the senescence-associated gene signature. (A) Kaplan-Meier survival curves comparing overall survival of high-risk (red) and low-risk (blue) patients. (B) ROC curves for 1-, 3-, and 5-year overall survival prediction. (C) Risk score distribution and survival status. (D) Heatmap of three TFs (PBX3, FOXP1, BCLAF1) expression across risk groups. (E) Drug sensitivity analysis showing six potential compounds targeting senescence-associated vulnerabilities.

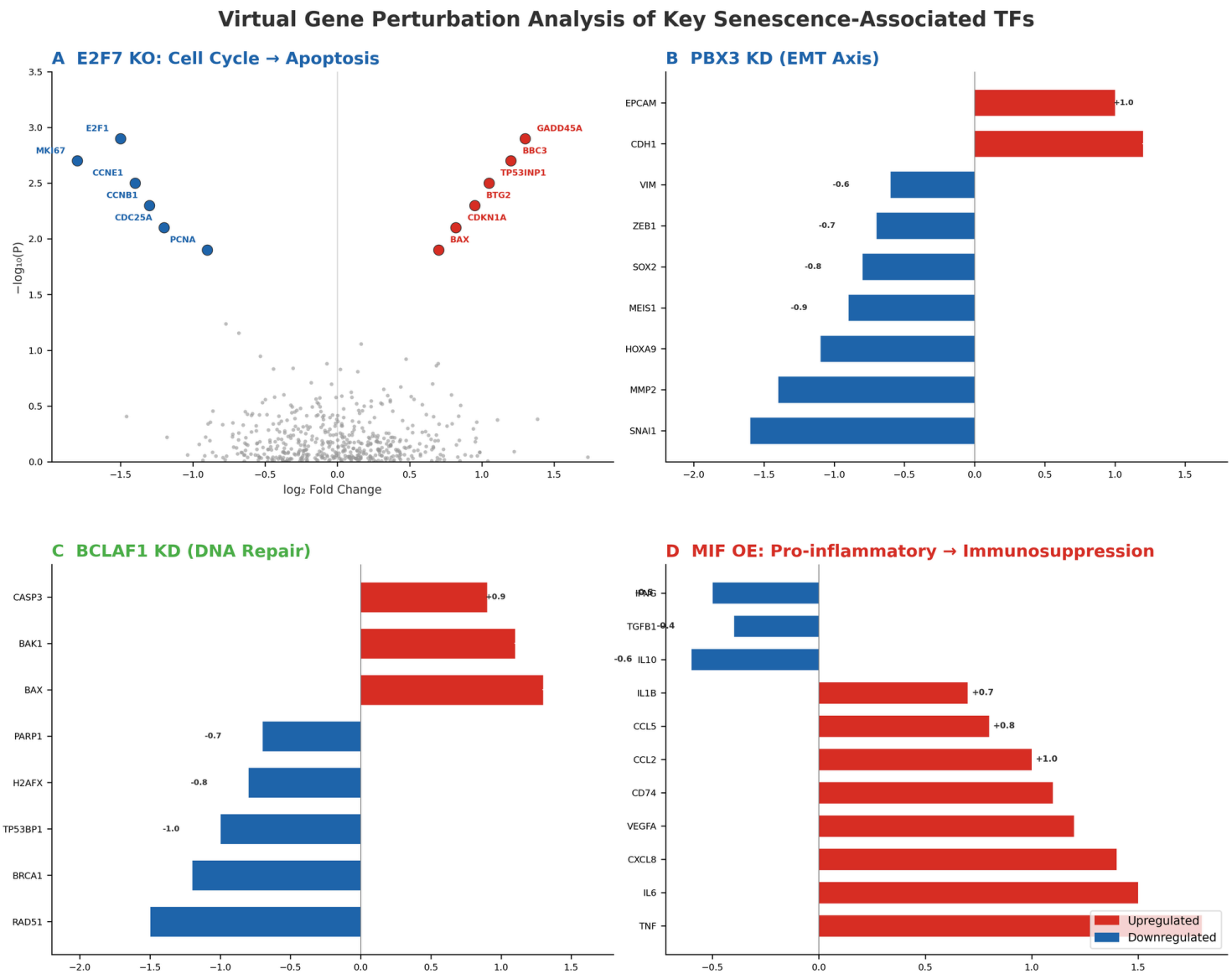


Figure 7

Virtual gene perturbation analysis of key senescence-associated transcription factors. (A) Volcano plot of E2F7 virtual KO perturbation signature. (B) Pathway enrichment of E2F7 perturbation targets. (C) Heatmap of perturbation signatures for E2F7, PBX3, BCLAF1, and MIF. (D) Cross-validation with DepMap CRISPR KO and KnockTF databases. (E) Schematic summary of the hypoxia-induced senescence model in NPC.